Rate Constants for the Reactions of a Series of Alkylperoxy Radicals with NO

Jia-Hua Xing and Akira Miyoshi*

Department of Chemical System Engineering, The University of Tokyo, 7-3-1 Hongo, Bunkyo-ku, Tokyo 113-8656, Japan

Received: February 3, 2005; In Final Form: March 24, 2005

The rate constants for the gas-phase reactions of isopropyl- and *tert*-butylperoxy radicals with nitric oxide (NO) have been studied at 298 ± 2 K and a total pressure of 3−4 Torr (He buffer) using a laser flash photolysis technique coupled with a time-resolved negative-ionization mass spectrometry. The alkyl peroxy radicals were generated by the reaction of alkyl radicals with excess O_2, where alkyl radicals were prepared by laser photolysis of several precursor molecules. The rate constants were determined to be $k(i\text{-}C_3H_7O_2 + NO) = (8.0 \pm 1.5) \times 10^{-12}$ and $k(t\text{-}C_4H_9O_2 + NO) = (8.6 \pm 1.4) \times 10^{-12}$ cm^3 molecule^{-1} s^{-1}. The results in combination with our previous studies are discussed in terms of the systematic reactivity of alkyl peroxy radicals toward NO.

1. Introduction

The reactions of organic peroxy radicals (RO_2) with nitric oxide (NO) play an important role in the atmospheric photooxidation of organic compounds, as a dominant oxidation process of NO in the polluted air.

$$RO_2 + NO \rightarrow RO + NO_2 \qquad (1)$$

As was reviewed by King et al.,[1] numerous studies have been reported for the reactions of organic peroxy radicals with NO. There is a recognizable trend that peroxy radicals with halogen substituents have larger rate constants for the reaction with NO. Kings et al.[1] indicated that substitution on peroxy radicals with electron-withdrawing groups such as halogen atoms increases the rate constant, and on the contrary, substitution with electron-donating groups such as alkyl groups decreases the rate constant. However, the question as to whether the alkyl substitution decreases the rate constant or not is still controversial.

Systematic studies on the RO_2 + NO reactions for a series of alkylperoxy radicals have been reported by a few groups. Adachi and Basco[2] have studied the reactions of methyl-, ethyl-, and isopropylperoxy radicals, and no significant difference was found among the rate constants. Peeters et al.[3] have studied the $i\text{-}C_3H_7O_2$ + NO and the $t\text{-}C_4H_9O_2$ + NO reactions and suggested that increasing of CH_3 substituents decreases the rate constant, which was also supported by the study of Sehested et al.,[4] who reported the rate constants for the alkylperoxy radicals CH_3O_2, $C_2H_5O_2$, $(CH_3)_3CCH_2O_2$, and $(CH_3)_3CC(CH_3)_2CH_2O_2$. On the other hand, Eberhard and Howard[5] have concluded that the rate constants for the reactions of NO with saturated aliphatic peroxy radicals can be approximated to be nearly identical, ∼8×10^{-12} cm^3 molecule^{-1} s^{-1}, from the studies of RO_2 + NO reactions for a series of alkylperoxy radicals by the technique of a flow tube reactor combined with chemical ionization mass spectrometry for the detection of RO_2.

The rate constants for isopropyl- and *tert*-butylperoxy radicals reported by Eberhard and Howard[5] are about a factor of 2 higher than those reported by Peeters et al.[3] Eberhard and Howard[5] discussed that the studies by Peeters et al.[3] and Sehested et al.[4] were likely to have suffered from fragmentation and secondary chemistry with the large alkyl groups because the rate constants were derived from the rate of appearance of the NO_2 product. The discrepancy should be resolved by further experimental studies.

In this study, the rate constants for the reactions

$$i\text{-}C_3H_7O_2 + NO \rightarrow \text{products} \qquad (2)$$

$$t\text{-}C_4H_9O_2 + NO \rightarrow \text{products} \qquad (3)$$

were investigated by using a laser flash photolysis coupled with time-resolved negative-ionization mass spectrometry technique for the detection of alkylperoxy radicals. A systematic trend in the rate constants will be discussed on the basis of the experimental results with our previous studies[6] on the reactions of NO with methyl- and ethylperoxy radicals.

2. Experimental Section

Apparatus. The experimental setup of the laser flash photolysis coupled with negative-ionization mass spectrometry (NIMS) has been described previously in the kinetic studies on the reactions of methyl- and ethylperoxy radicals with NO[6] and is described only briefly here. The reactant gas mixture diluted in helium was flowed into a tubular Pyrex reaction cell and was irradiated by an ArF (193 nm) or a KrF (248 nm) excimer laser introduced coaxially into the cell. The reacting gases were sampled through a 200 μm pinhole located on the wall at the distance of 45 cm from the inlet port and were led into the ionization chamber.

Alkylperoxy radicals were negatively ionized by the electron transfer from high-Rydberg state of xenon gas atoms (Xe**).

$$Xe^{**} + RO_2 \rightarrow Xe^+ + RO_2^- \qquad (4)$$

The principle of the ionization method has been described by Kondow.[7] Gaseous xenon was continuously introduced into the electron-impact tube attached to the ionization chamber and was

* To whom correspondence should be addressed. E-mail: miyoshi@chemsys.t.u-tokyo.ac.jp.

10.1021/jp050609s CCC: $30.25
Published on Web 04/20/2005

TABLE 1: Reactions and Rate Constants Used in the Numerical Simulations for the Measurements of the *i*-$C_3H_7O_2$ + NO Reaction[a]

no.	reaction	k (298 K, 4 Torr)	reference
ip1	i-$C_3H_7 + O_2 + M \rightarrow i$-$C_3H_7O_2 + M$	1.41×10^{-11}	15
ip2	i-$C_3H_7O_2 + NO \rightarrow i$-$C_3H_7O + NO_2$	8.1×10^{-12}	this work
ip3	i-$C_3H_7O_2 \rightarrow$ (wall loss reaction)	4.0 (s^{-1})	this work
ip4	i-$C_3H_7O_2 + i$-$C_3H_7O_2 \rightarrow 2C_3H_7O + O_2$	5.6×10^{-16}	16
ip5	i-$C_3H_7O_2 + i$-$C_3H_7O_2 \rightarrow CH_3COCH_3 + C_3H_7OH + O_2$	4.4×10^{-16}	16
ip6	i-$C_3H_7O_2 + NO_2 \rightarrow i$-$C_3H_7O_2NO_2$	3.0×10^{-12}	this work
ip7	i-$C_3H_7O_2 + HO_2 \rightarrow i$-$C_3H_7OOH + O_2$	8.0×10^{-12}	estimated[b]
ip8	i-$C_3H_7 + i$-$C_3H_7 \rightarrow C_3H_6 + C_3H_8$	4.25×10^{-12}	17
ip9	i-$C_3H_7 + i$-$C_3H_7 \rightarrow C_6H_{14}$	6.64×10^{-12}	17
ip10	i-$C_3H_7O \rightarrow CH_3 + CH_3CHO$	1.46×10^{2} (s^{-1})	18
ip11	i-$C_3H_7O + O_2 \rightarrow CH_3COCH_3 + HO_2$	6.9×10^{-15}	16
ip12	i-$C_3H_7O + NO + M \rightarrow i$-$C_3H_7ONO + M$	8.9×10^{-12}	19
ip13	i-$C_3H_7O + NO \rightarrow HNO + CH_3COCH_3$	6.51×10^{-12}	16
ip14	i-$C_3H_7O + NO_2 + M \rightarrow i$-$C_3H_7ONO_2 + M$	3.5×10^{-11}	20
ip15	$CH_3 + O_2 + M \rightarrow CH_3O_2 + M$	4.8×10^{-14}	8
ip16	$CH_3O_2 + NO \rightarrow CH_3O + NO_2$	9.9×10^{-11}	6
ip17	$HO_2 + NO \rightarrow OH + NO_2$	8.1×10^{-12}	8
ip18	$2HO_2 \rightarrow H_2O_2 + O_2$	5.9×10^{-15}	8
ip19	$HO_2 + NO_2 + M \rightarrow HO_2NO_2 + M$	2.2×10^{-14}	8
ip20	$HO_2 + OH \rightarrow H_2O + O_2$	1.1×10^{-10}	8
ip21	$OH + OH + M \rightarrow H_2O_2 + M$	8.3×10^{-14}	8
ip22	$OH + NO + M \rightarrow HONO + M$	8.5×10^{-14}	8
ip23	$OH + NO_2 + M \rightarrow HNO_3 + M$	2.8×10^{-13}	8
ip24	$OH + CH_3COCH_3 \rightarrow CH_3COCH_2 + H_2O$	1.8×10^{-13}	21
ip25	$OH + i$-$C_3H_7OH \rightarrow C_3H_6OH + H_2O$	5.1×10^{-12}	16
ip26	$C_3H_6OH + O_2 \rightarrow HOC_3H_6O_2$	1.2×10^{-11}	22
ip27	$HOC_3H_6O_2 + NO \rightarrow HOC_3H_6O + NO_2$	1.0×10^{-11}	estimated
ip28	$2NO + O_2 \rightarrow 2NO_2$	1.9×10^{-38} (cm^6 $molecule^{-2}$ s^{-1})	16
	Reactions for Experiments by Using Isopropyl Bromide		
ip29	i-$C_3H_7 + BR \rightarrow C_3H_6 + HBR$	1.18×10^{-11}	estimated[b]
ip30	$BR + BR + M \rightarrow BR_2 + M$	4.1×10^{-16}	23
ip31	$BR + NO + M \rightarrow BRNO + M$	1.23×10^{-14}	24
ip32	$BR + NO_2 + M \rightarrow BRNO_2 + M$	5.1×10^{-14}	8
ip33	$BR_2 + OH \rightarrow HOBR + BR$	4.2×10^{-11}	8
ip34	$HO_2 + BR \rightarrow HBR + O_2$	2.0×10^{-12}	8
	Reactions for Experiments by Using Isopropyl Iodide		
ip35	i-$C_3H_7 + I \rightarrow C_3H_6 + HI$	1.18×10^{-11}	estimated[b]
ip36	$I + NO + M \rightarrow INO + M$	2.3×10^{-15}	16
ip37	$I + NO_2 + M \rightarrow INO_2 + M$	3.8×10^{-15}	16
ip38	$INO + INO \rightarrow I_2 + 2NO$	1.3×10^{-14}	8, 16
ip39	$INO_2 + INO_2 \rightarrow I_2 + 2NO_2$	4.7×10^{-15}	8, 16
ip40	$I_2 + OH \rightarrow HOI + I$	1.79×10^{-10}	8, 16

[a] The rate constants are for 298 K and 4 Torr (He buffer) condition in unit of cm^3 $molecule^{-1}$ s^{-1}. [b] The value for C_2H_5.

excited to high-Rydberg states (Xe**) by collision with accelerated electrons released from a helical filament.

Reactant Preparation. The isopropyl- or *tert*-butylperoxy radicals were generated by reacting isopropyl radicals ((3.4−18) × 10^{12} molecules cm^{-3}) or *tert*-butyl radicals ((1.4−15) × 10^{12} molecules cm^{-3}), respectively, with excess O_2 diluted in He. The isopropyl and *tert*-butyl radicals were produced by 193 nm laser photolysis of respective bromides or by 248 nm photolysis of respective iodides.

$$RX + h\nu \rightarrow R + X \ (X = Br \text{ or } I) \qquad (5)$$

$$R + O_2 + M \rightarrow RO_2 + M \qquad (6)$$

The NO concentration was varied within the range where the reaction of RO_2 + NO could be observed in a time scale of 3−25 ms. The oxidation of NO by the reaction of $2NO + O_2 \rightarrow 2NO_2$ was negligible under the experimental conditions.

Experimental Conditions and Data Analysis. Kinetic measurements were carried out at laser repetition rate of 11−12 Hz with flow velocity in the reaction cell of ∼13 m s^{-1} to ensure complete replenishment of gas samples between successive laser shots. The ion signals were collected at the gate width of 50−100 μs and were accumulated over 20 000−30 000 laser shots in order to obtain a temporal profile of RO_2 concentrations. Temporal profiles of the ion signal were recorded from 20 ms before to 30 ms after the photolysis laser pulse. The fluence of the laser light was in the range 3−11 mJ cm^{-2} $pulse^{-1}$ for 193 nm and 16−20 mJ cm^{-2} $pulse^{-1}$ for 248 nm.

The initial concentration of alkylperoxy radicals was evaluated from the precursor concentration and the laser fluence assuming the quantitative conversion from alkyl radicals generated by photolysis. The yields of alkyl radicals from 193 nm photolysis of bromides were determined from the separate experiments as described later. Those from 248 nm photolysis of iodides were derived from the absorption cross section (σ) and the photolysis quantum yield (Φ) from the JPL Evaluation No. 14.[8] The concentration of O_2 was maintained in the range of 0.4−0.6 Torr in order to ensure the instantaneous conversion of alkyl radicals to alkylperoxy radicals, within 0.1 ms, compared to the time scale of the reaction of interest. Because there is a tradeoff relation between the detection sensitivity and the detection time resolution, near the lowest allowable time resolution was chosen. Analyses were accordingly made in the range from 3 to 12−25 ms after the laser photolysis, depending on the decay time constant. Experiments were carried out at room temperature (298 ± 2 K) and total pressure of 3−4 Torr maintained by helium.

The detection limits of isopropylperoxy and *tert*-butylperoxy radicals were 1.5 × 10^{12} and 8.7 × 10^{11} molecules cm^{-3}, respectively, at 2.0 s acquisition time. The rate constants for

TABLE 2: Reactions and Rate Constants Used in the Numerical Simulations for the Measurements of *t*-$C_4H_9O_2$ + NO Reaction[a]

no.	reaction	k (298 K, 4 Torr)	reference
tb1	t-$C_4H_9 + O_2 \rightarrow t$-$C_4H_9O_2$	2.34×10^{-11}	25
tb2	t-$C_4H_9O_2 + NO \rightarrow t$-$C_4H_9O + NO_2$	8.6×10^{-12}	this work
tb3	t-$C_4H_9O_2 \rightarrow$ (wall loss reaction)	4.0 (s^{-1})	this work
tb4	t-$C_4H_9O_2 + t$-$C_4H_9O_2 \rightarrow 2t$-$C_4H_9O + O_2$	2.6×10^{-17}	17
tb5	t-$C_4H_9O_2 + NO_2 \rightarrow t$-$C_4H_9O_2NO_2$	1.5×10^{-12}	this work
tb6	t-$C_4H_9O_2 + HO_2 \rightarrow t$-$C_4H_9OOH + O_2$	8.0×10^{-12}	estimated[b]
tb7	t-$C_4H_9 + t$-$C_4H_9 \rightarrow i$-$C_4H_8 + i$-C_4H_{10}	2.24×10^{-11}	26
tb8	t-$C_4H_9 + t$-$C_4H_9 \rightarrow C_8H_{18}$	7.77×10^{-12}	26
tb9	t-$C_4H_9O \rightarrow CH_3 + CH_3COCH_3$	8.01×10^{2} (s^{-1})	18
tb10	t-$C_4H_9O + NO \rightarrow t$-$C_4H_9ONO$	3.32×10^{-11}	estimated[c]
tb11	t-$C_4H_9O + NO_2 \rightarrow t$-$C_4H_9ONO_2$	5.47×10^{-13}	27
tb12	$CH_3 + O_2 + M \rightarrow CH_3O_2 + M$	4.8×10^{-14}	8
tb13	$CH_3O_2 + NO \rightarrow CH_3O + NO_2$	9.9×10^{-11}	6
tb14	$HO_2 + NO \rightarrow OH + NO_2$	8.1×10^{-12}	8
tb15	$2HO_2 \rightarrow H_2O_2 + O_2$	5.9×10^{-15}	8
tb16	$HO_2 + NO_2 + M \rightarrow HO_2NO_2 + M$	2.2×10^{-14}	8
tb17	$HO_2 + OH \rightarrow H_2O + O_2$	1.1×10^{-10}	8
tb18	$OH + OH + M \rightarrow H_2O_2 + M$	8.3×10^{-14}	8
tb19	$OH + NO + M \rightarrow HONO + M$	8.5×10^{-14}	8
tb20	$OH + NO_2 + M \rightarrow HNO_3 + M$	2.8×10^{-13}	8
tb21	$OH + t$-$C_4H_9 \rightarrow H_2O + C_4H_8$	3.01×10^{-11}	28
tb22	$OH + CH_3COCH_3 \rightarrow CH_3COCH_2 + H_2O$	1.8×10^{-13}	21
tb23	$2NO + O_2 \rightarrow 2NO_2$	1.9×10^{-38} (cm^6 $molecule^{-2}$ s^{-1})	16
	Reactions for Experiments Using *tert*-Butyl Bromide		
tb24	t-$C_4H_9 + BR \rightarrow C_4H_8 + HBR$	1.18×10^{-11}	estimated[b]
tb25	$BR + BR + M \rightarrow BR_2 + M$	4.1×10^{-16}	23
tb26	$BR + NO + M \rightarrow BRNO + M$	1.23×10^{-14}	24
tb27	$BR + NO_2 + M \rightarrow BRNO_2 + M$	5.1×10^{-14}	8
tb28	$BR_2 + OH \rightarrow HOBR + BR$	4.2×10^{-11}	8
tb29	$HO_2 + BR \rightarrow HBR + O_2$	2.0×10^{-12}	8
	Reactions for Experiments by Using *tert*-Butyl Iodide		
tb30	t-$C_4H_9 + I \rightarrow C_4H_8 + HI$	1.16×10^{-11}	estimated[b]
tb31	$I + NO + M \rightarrow INO + M$	2.3×10^{-15}	16
tb32	$I + NO_2 + M \rightarrow INO_2 + M$	3.8×10^{-15}	16
tb33	$INO + INO \rightarrow I_2 + 2NO$	1.3×10^{-14}	8, 16
tb34	$INO_2 + INO_2 \rightarrow I_2 + NO_2$	4.70×10^{-15}	8, 16
tb35	$I_2 + OH \rightarrow HOI + I$	1.79×10^{-10}	8, 16

[a] The rate constants are for 298 K and 4 Torr (He buffer) condition in unit of cm^3 $molecule^{-1}$ s^{-1}. [b] The value for C_2H_5. [c] The value for isobutyl and *n*-butyl.

the reactions 2 and 3 were determined by kinetic models with all considerable reactions occurring in the reaction systems using Chemkin-II,[9] though some of the reactions considered are eventually negligible. The reactions considered are listed in Table 1 and Table 2. The model was run for each experiment, and the rate constant was derived by using the least-squares analysis by fitting with the model.

Determination of the Alkyl Radical Yields from the Photolysis. As neither absorption cross section nor photolysis quantum yield for isopropyl or *tert*-butyl bromides has been reported, the alkyl radical yields were determined experimentally by NO_2 titration. The experiment was performed by using a photoionization mass spectrometer (PIMS) coupled with laser flash photolysis, which has been described elsewhere.[10] The alkyl radicals generated after the photolysis of alkyl bromides were converted to NO by the reaction with excess NO_2, which was introduced into the reactor together with the bromide.

$$RBr + h\nu \rightarrow R + Br \quad (5)$$

$$R + NO_2 \rightarrow RO + NO \quad (7)$$

The amount of NO produced was assumed to be equal to that of alkyl radicals. At 193 nm, some of the NO_2 also photolyzed to generate NO.

$$NO_2 + h\nu \rightarrow NO + O \quad (8)$$

To minimize this influence, the laser fluence was kept as low as ca. 2 mJ cm^{-2} $pulse^{-1}$. Nevertheless, a small production of NO from the photolysis of NO_2 was corrected by subtraction of NO^+ signal observed without RBr. A hydrogen resonance lamp (10.2 eV) was used for the ionization of NO. Typical concentration of NO_2 was 5.5−7.5 mTorr and was about 300 times larger than that of alkyl radicals.

To avoid systematic error, the NO_2 titration experiment was performed for isopropyl, *tert*-butyl, and ethyl bromides. The results of isopropyl and butyl bromides were compared with that of ethyl bromide, for which photochemical data[11,12] are available.

Determination of the Rate Constants for the Reactions of RO_2 with Nitrogen Dioxides. Since the reactions of RO_2 with nitrogen dioxides (reaction ip6 in Table 1 and reaction tb5 in Table 2)

$$RO_2 + NO_2 + M \rightarrow RO_2NO_2 + M \quad (9)$$

were found to affect the measurements for $RO_2 + NO$, the rate constants for these reactions were also determined at the same total pressure, 4 Torr, as for $RO_2 + NO$ experiments. In these experiments RO_2 was generated by the 248 nm photolysis of the corresponding alkyl iodide because photodissociation of NO_2 is significant at 193 nm but negligible at 248 nm. Similar to the measurements of $RO_2 + NO$, all the reactants were

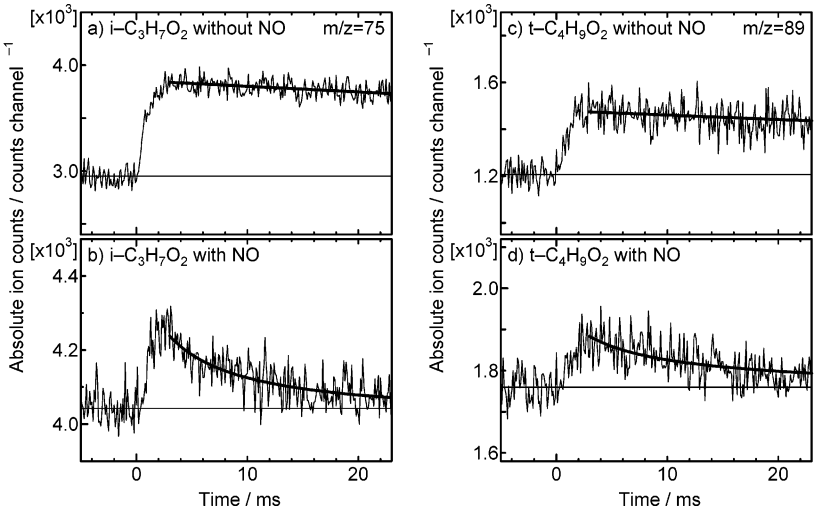

Figure 1. Typical temporal profiles of i-$C_3H_7O_2^-$ and t-$C_4H_9O_2^-$. Experimental conditions: (a) [i-$C_3H_7O_2$] = 4.6×10^{12} molecules cm^{-3}, [NO] = 0; (b) [i-$C_3H_7O_2$] = 1.8×10^{13}, [NO] = 2.2×10^{13} molecules cm^{-3}; (c) [t-$C_4H_9O_2$] = 1.8×10^{12} molecules cm^{-3}, [NO] = 0; (d) [i-$C_4H_9O_2$] = 1.3×10^{13}, [NO] = 1.7×10^{13} molecules cm^{-3}. The thick lines are pseudo-first-order fittings for (a) and (c) and model fittings for (b) and (d), which all start from 3 ms after the laser flash.

introduced into the reaction cell, and the decay of RO_2 signals was monitored. RO_2 concentration was in the range $(2-4) \times 10^{12}$ molecules cm^{-3}. The analysis was done by second-order rate fitting and by using the model with same reactions as used for RO_2 + NO analysis.

Materials. The following gases and reagents were used without further purification: helium (Nippon Sanso, 99.9999%), O_2 (Nippon Sanso, 99.99%), NO/He (Nippon Sanso, 5.48%), i-C_3H_7Br (Tokyo Kasei, >99%), t-C_4H_9Br (Tokyo Kasei, >99%), C_2H_5Br (Tokyo Kasei, >99%), i-C_3H_7I (Tokyo Kasei, >98%), and t-C_4H_9I (Tokyo Kasei, >95%). All the liquid samples were deaerated by several freeze−pump−thaw cycles before use. NO_2 was prepared by mixing pure NO gas (Matheson) with stoichiometrically excess O_2 and diluted in He before use.

3. Results

Typical temporal profiles of the signals at m/z = 75 (i-$C_3H_7O_2^-$) and m/z = 89 (t-$C_4H_9O_2^-$) are shown in Figure 1. Because the alkyl radicals were produced by the photolysis of the alkyl halides, other structural isomers of alkylperoxy radicals were unlikely present in the experimental system. Because the detection sensitivities were relatively low for these two peroxy radicals, the pseudo-first-order condition was unable to be assumed. At first, the analyses were made using the second-order formula:

$$[RO_2] = \frac{\alpha}{\beta \exp(\alpha k t) - 1} \qquad \text{(E1)}$$

$$\alpha = [NO]_0 - [RO_2]_0, \quad \beta = [NO]_0/[RO_2]_0$$

where k is the overall rate constant for the reaction of either i-$C_3H_7O_2$ + NO or t-$C_4H_9O_2$ + NO.

In the detailed analysis using the kinetic model including the side reactions, the derived rate constants were smaller than those by assuming the second-order condition. It is recognized that the interference of the reaction of alkylperoxy radicals with NO_2 (reactions ip6 and tb5 in Tables 1 and 2, respectively)

$$RO_2 + NO_2 (+M) \rightarrow RO_2NO_2 (+M) \qquad (7)$$

was not negligible in both experiments for i-$C_3H_7O_2$ and t-$C_4H_9O_2$. A result of sensitivity analysis for the i-$C_3H_7O_2$ + NO measurement is shown in Figure 2. The second-order rate constants for reaction 7 were evaluated to be $k_7(i\text{-}C_3H_7O_2) = (3.0 \pm 1.6) \times 10^{-12}$ and $k_7(t\text{-}C_4H_9O_2) = (1.5 \pm 0.8) \times 10^{-12}$ cm^3 molecule^{-1} s^{-1} at total pressure of 4 Torr maintained by He. The specified uncertainty limits are 2σ of the measurements.

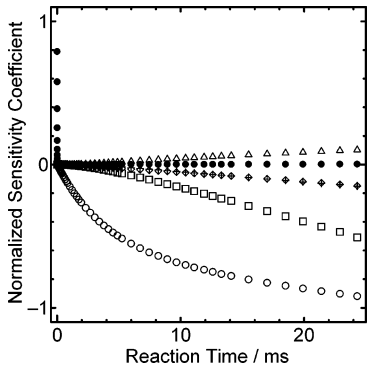

Figure 2. Plots of the normalized sensitivity coefficients, (k_i/[i-$C_3H_7O_2$]) (∂[i-$C_3H_7O_2$]/∂k_i), for i-$C_3H_7O_2$ concentration, [i-$C_3H_7O_2$], with respect to the important reaction rate constants, k_i. The symbols and the corresponding reactions are as follows: (○) i-$C_3H_7O_2$ + NO → i-C_3H_7O + NO_2 (ip2 in Table 1); (□) i-$C_3H_7O_2$ + NO_2 + M → i-$C_3H_7O_2NO_2$ + M (ip7); (+) i-C_3H_7O + O_2 → CH_3COCH_3 + HO_2 (ip12); (◇) $C_3H_7O_2$ → heterogeneous loss (ip4); (△) i-C_3H_7O + NO + M → i-C_3H_7ONO + M (ip13); (●) i-C_3H_7 + O_2 + M → i-$C_3H_7O_2$ + M (ip1). Sensitivity coefficients were calculated by the CHEMKIN II, SENKIN program,[9] for the experimental conditions corresponding to Figure 1b.

The numerical analyses were conducted for all of the experiment results. The derived rate constants for i-$C_3H_7O_2$ + NO (2) were 7.9×10^{-12} and 8.3×10^{-12} cm^3 molecule^{-1} s^{-1} when using bromide and iodide as precursor, respectively. Similarly for t-$C_4H_9O_2$ + NO (3) the rate constants were 8.8×10^{-12} and 8.5×10^{-12} cm^3 molecule^{-1} s^{-1} with bromide and iodide, respectively. The best-fit numerical simulation results were also shown in Figure 1b,d. The rate constants measured with different precursors well agreed with each other. Consequently, the determined rate constants in this study were $k_2 = (8.0 \pm 1.5) \times 10^{-12}$ and $k_3 = (8.6 \pm 1.4) \times 10^{-12}$ cm^3 molecule^{-1} s^{-1} for the i-$C_3H_7O_2$ + NO and the t-$C_4H_9O_2$ + NO reactions, respectively, as the average of 12 and 10 experiments in total, respectively. The error limit given above

TABLE 3: Summary of Room Temperature Measurements of the Rate Constants for RO_2 + NO Reactions (RO_2 = Alkylperoxy)

	$k/10^{-12}$ cm^3 molecule^{-1} s^{-1}				
RO_2	ref 2	ref 3	ref 4	ref 5[a]	this work[b]
CH_3O_2	3.0 ± 0.2		8.8 ± 1.4	7.5 ± 1.3	9.9 ± 2.1
$C_2H_5O_2$	2.7 ± 0.2		8.5 ± 1.2	9.3 ± 1.6	11.0 ± 0.8
n-$C_3H_7O_2$				9.4 ± 1.6	
i-$C_3H_7O_2$	3.5 ± 0.2	5.0 ± 1.2		9.1 ± 1.5	8.0 ± 1.3
t-$C_4H_9O_2$		4.0 ± 1.1		7.9 ± 1.3	8.6 ± 1.4
neo-$C_5H_{11}O_2$			4.7 ± 0.4		
$(CH_3)_3C-C(CH_3)_2CH_2O_2$			1.8 ± 0.2		
observed species	RO_2	NO_2	NO_2	RO_2	RO_2
method[c]	UVA	DF-EIMS	PR-UVA	FT-CIMS	LP-NIMS

[a] Including the other studies reported by the same group. [b] The rate constants for CH_3O_2 and $C_2H_5O_2$ are from our previous work.[6] [c] UVA = ultraviolet absorption, EIMS = electron impact mass spectrometry, LP = laser photolysis, PR = pulse radiolysis, DF = discharge flow, CIMS = chemical ionization mass spectrometry, FT = flow tube.

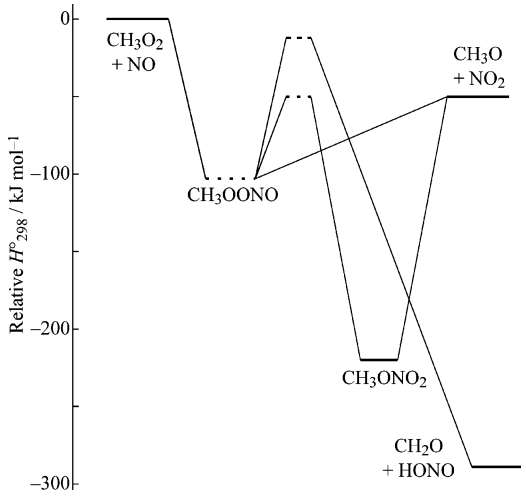

Figure 3. Estimated energy diagram for the reaction of CH_3O_2 + NO. Dotted lines (···) denote estimation by G3(MP2)//B3LYP, while the solid lines (—) were calculated from experimental heats of formation at 298 K.

represents the overall error in the rate constant considering the propagation of uncertainties in the concentration of precursors, the photolysis laser intensity, the photochemical data, and the uncertainty in the measured rate constants of the reaction RO_2 + NO_2.

4. Discussion

In Table 3, the results of our present and previous studies are compared with those available in the literature. Here, to avoid the complexity arising from the systematic errors, only those that have been investigated by the same group were listed, though the rate constants for the reactions of CH_3O_2 and $C_2H_5O_2$ with NO have been the subjects of a number of other previous studies.

In the present study, the rate constants for isopropyl- and *tert*-butylperoxy radicals were found to be significantly smaller than that for ethylperoxy radical, though some previous studies suggested nearly equal rate constants for RO_2 + NO irrespective of the difference of alkyl group. In this section, the reactivity of RO_2 with NO will be discussed in relation to the structures and energetics of alkyl peroxy radicals and peroxynitrite intermediates.

Figure 3 shows the estimated energy diagram for CH_3O_2 + NO reaction. Energies for CH_3OONO and the transition states were estimated by quantum chemical calculation, G3(MP2)//B3LYP theory,[13] done by Gaussian 03.[14] Although the reaction is expected to proceed via CH_3OONO complex formation at the first stage, existence of the low-energy exit channel to CH_3O + NO_2 makes this reaction essentially pressure-independent because of the much larger dissociation rate constant of energized complex, CH_3OONO^*, to CH_3O + NO_2 than that for the backward dissociation to CH_3O_2 + NO. As has been known experimentally, the existence of the isomerization channel to $RONO_2$ suggests the pressure enhancement of product branching fraction to $RONO_2$, especially for large RO_2. For this type of reaction, the rate constant for the disappearance of the reactants is most likely to be controlled by the transition state at the entrance channel, though no pronounced barrier is expected for this simple bond fission reaction.

TABLE 4. Estimated Thermodynamic Functions for RO_2 + NO → ROONO

RO_2	ΔE°_0[a]/ kJ mol^{-1}	ΔH°_{298}/ kJ mol^{-1}	ΔS°_{298}/ J K^{-1} mol^{-1}	ΔG°_{298}/ kJ mol^{-1}
CH_3O_2	−99.74	−103.09	−156.36	−56.42
$C_2H_5O_2$	−100.64	−103.09	−155.05	−56.81
i-$C_3H_7O_2$	−100.29	−103.30	−159.40	−55.72
t-$C_4H_9O_2$	−99.04	−102.33	−159.51	−54.78

[a] Calculated from G3(MP2)//B3LYP E(0K)'s for the most stable conformer. Thermodynamic functions were calculated by using the properties listed in Table 5.

Kings et al.[1] have discussed the reactivity of RO_2 with NO in terms of their SOMO (singly occupied molecular orbital) energies. They showed that the difference of SOMO energies between two reactants, NO and peroxy radical, correlates the rate constant. Because it is often expected that the closer the SOMO energies, the larger is the bonding interaction, such an effect would also be reflected in the bond dissociation energies, which will be a more quantitative measure for this effect. Therefore, quantum chemical calculations were made for RO_2, NO, and ROONO in the present study, to compare the thermodynamics of these species. The direct quantum-chemical probing of the entrance region of RO_2 + NO → ROONO, which will require a high-level of the MRCI (multireference configuration interaction) method, seems to be beyond the scope of the present study.

The estimated thermodynamic functions for the reactions

$$RO_2 + NO \rightarrow ROONO \qquad (10)$$

(R = CH_3, C_2H_5, *i*-C_3H_7, and *t*-C_4H_9) are listed in Table 4. Despite the trend estimated from the SOMO energy differences,[1] the bond dissociation energies ($-\Delta E^\circ_0$ or $-\Delta H^\circ_{298}$) are almost equal for all reactions, and no systematic relation with the rate constant was found. On the other hand, a good correlation was found between the rate constant and the reaction entropy, ΔS°_{298}, as plotted in Figure 4.

TABLE 5: Molecular Properties Used in the Thermodynamic Calculations

species	NO	CH_3O_2	CH_3OONO	$C_2H_5O_2$	C_2H_5OONO
m^a/amu	29.998	47.013	77.011	61.029	91.027
g (ϵ/cm^{-1})^b	2, 2(119.73)	2	1	2	1
n (ϵ/cm^{-1})^c	1	1	2, 2(468.7)	2, 1(4.5)	2, 2(85.9), 2(116.1), 2(468.7), 2(554.6), 2(584.8)
σ^d	1	1	1	1	1
A, B, C^e/cm^{-1}	1.6817	1.7353, 0.3772, 0.3296	0.4000, 0.1303, 0.1127	0.5905, 0.1877, 0.1620	0.3035, 0.0692, 0.0618
ν^f/cm^{-1}	1914	474, 891, 1095, 1124, 1181, 1405, 1442, 1453, 2957, 3046, 3059	280, 326, 473, 511, 765, 903, 979, 1135, 1171, 1414, 1438, 1474, 1713, 2934, 3010, 3030	346, 509, 775, 820, 967, 1066, 1121, 1168, 1267, 1338, 1378, 1450, 1457, 1474, 2946, 2968, 3011, 3018, 3036	222, 308, 372, 472, 510, 792, 807, 871, 908, 999, 1119, 1151, 1244, 1355, 1387, 1454, 1472, 1494, 1709, 2936, 2948, 2978, 3017, 3026
B:V_0 (σ)^g/ cm^{-1}		7.0457:286(3)	1.1124:1420(2), 5.4536:738(3)	2.2207:655(3), 5.6526:1098(3)	0.8742:706(3), 0.9359:1757(2), 5.5355:1132(3)
E_0^h/hartrees	−129.758098	−189.977933	−319.774020	−229.219311	−359.015739

species	i-$C_3H_7O_2$	i-C_3H_7OONO	t-$C_4H_9O_2$	t-C_4H_9OONO
m^a	75.045	105.043	89.06	119.058
g (ϵ)^b	2	1	2	1
n (ϵ)^c	2, 1(142)	2, 2(55.8), 2(291.8), 2(468.7), 2(524.5), 2(760.5)	1	2, 2(468.7)
σ^d	1	1	1	1
A, B, C^e	0.2630, 0.1351, 0.0982	0.1657, 0.0574, 0.0477	0.1489, 0.0959, 0.0959	0.1187, 0.0461, 0.0430
ν^f	290, 329, 436, 504, 769, 861, 912, 923, 1094, 1121, 1162, 1170, 1304, 1328, 1372, 1389, 1452, 1458, 1463, 1479, 2941, 2945, 2968, 3006, 3015, 3019, 3028	213, 286, 345, 368, 469, 484, 513, 781, 822, 883, 904, 912, 927, 1103, 1136, 1166, 1319, 1338, 1376, 1389, 1451, 1458, 1464, 1481, 1708, 2939, 2940, 2946, 3006, 3015, 3023, 3024	261, 319, 348, 388, 422, 525, 707, 780, 902, 904, 942, 1011, 1023, 1141, 1187, 1228, 1258, 1368, 1370, 1394, 1441, 1457, 1460, 1466, 1467, 1489, 2941, 2943, 2949, 3008, 3009, 3015, 3016, 3028, 3032	201, 253, 313, 338, 374, 402, 456, 490, 542, 722, 792, 831, 892, 902, 911, 941, 1017, 1024, 1181, 1232, 1248, 1370, 1372, 1396, 1442, 1457, 1459, 1467, 1470, 1489, 1704, 2941, 2943, 2949, 3007, 3010, 3017, 3019, 3023, 3024
B:V_0 (σ)^g	1.6903:653(3), 5.5222:849(3), 5.4238:1220(3)	0.5416:1504(2), 0.4711:1468(3), 5.3853:891(3), 5.3871:1221(3)	1.4495:1160(3), 5.4320:731(3), 5.3924:1151(3), 5.3924:1291(3)	0.4278:2301(2), 0.4093:1971(3), 5.3650:725(3), 5.3589:1192(3), 5.3680:1368(3)
E_0^h	−268.462903	−398.259198	−307.707131	−437.502951

[a] Mass of the molecule. [b] Degeneracy of the electronic state, with excitation energy in parentheses for excited state. [c] Number of optical isomers and rotational conformers, with its energy in parentheses for conformer with higher energy based on the calculated G3(MP2)//B3LYP E(0 K). [d] Rotational symmetry number. [e] Rotational constant derived from B3LYP/6-31G(d) optimized geometry. [f] B3LYP/6-31G(d) vibrational frequency scaled by 0.9613. [g] Sinusoidally hindered rotor parameters; B is the rotational constant for one-dimensional rotation, V_0 is the potential barrier, and σ is the symmetry number. [h] The ground-state energy of the most stable isomer based on the calculated G3(MP2)//B3LYP E(0 K).

The molecular properties, vibrational frequencies, rotational constants, hindered-rotor properties, etc., used in the thermodynamic calculations are listed in Table 5. Though the major part of the reaction entropy is the loss of translational entropy ($\sim$−17.6 in $\Delta S/R$), the difference of the reaction entropy, ΔS, among CH_3O_2, $C_2H_5O_2$, i-$C_3H_7O_2$, and t-$C_4H_9O_2$ is mainly caused by the difference of the hindrance of internal rotors of ROONO, especially the torsional rotations around C−O and O−O bonds. Although the fully quantitative understanding must be done with the VTST (variational transition-state theory) calculations on MRCI potential surface at the reaction entrance, similar hindrance of torsional motions in the transition-state region molecule can be reasonably assumed.

The negligible difference in the bond dissociation energy of ROONO to RO_2 + NO among different alkyl groups suggests the similarity of the potential energy surface in the entrance region. Thus, the major property controlling the rate constants for RO_2 + NO is suggested to be the entropy term, that is, the steric hindrance of the internal rotations for the case of R being saturated alkyl group. Since the electronic substitution effects

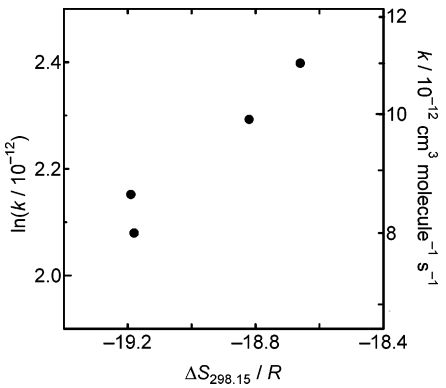

Figure 4. Correlation between the rate constant, k, for RO_2 + NO and the reaction entropy, ΔS, for RO_2 + NO → ROONO. The ordinate is in the scale of natural logarithm of k divided by 10^{-12} cm^3 molecule^{-1} s^{-1}. The right-side ordinate is corresponding antilog scale for reference.

implies the electronic effect on the potential energy term, the electron-donating effect of the CH_3 substitution does not seem to be significant for this reaction, though this does not reject the possibility of electron-withdrawing effects of halogen substitution. More experimental studies and precise quantum chemical calculations are needed to verify such a hypothesis.

5. Summary

The rate constants for the reactions of isopropyl- and *tert*-butylperoxy radicals with NO have been determined. The results together with our previous studies for methyl- and ethylperoxy radicals indicate a trend that the methyl substitution on α-carbon reduces the rate constant. A thermodynamic calculation based on the quantum chemical calculations shows that the rate constant correlates with the reaction entropy for $RO_2 + NO \rightarrow ROONO$. The steric hindrance caused by the methyl substitution is suggested to be the dominant factor that controlling the rate constant for $RO_2 + NO$ reactions.

Acknowledgment. This work was supported in part by a Grant-in-Aid from the Japanese Ministry of Education, Science, Sports, and Culture (No. 13640502 and priority field "Radical Chain Reactions").

References and Notes

(1) King, M. D.; Thompson, K. C. *Atmos. Environ.* **2003**, *37*, 4517.

(2) (a) Adachi, H.; Basco, N. *Chem. Phys. Lett.* **1979**, *63*, 490. (b) Adachi, H.; Basco, N. *Chem. Phys. Lett.* **1979**, *64*, 431. (c) Adachi, H.; Basco, N. *Int. J. Chem. Kinet.* **1982**, *14*, 1243.

(3) Peeters, J.; Vertommen, J.; Langhans, I. *Ber. Bunsen-Ges. Phys. Chem.* **1992**, *96*, 431.

(4) Sehested, J.; Nielsen, O. J.; Wallington, T. J. *Chem. Phys. Lett.* **1993**, *213*, 457.

(5) (a) Eberhard, J.; Howard, C. J. *Int. J. Chem. Kinet.* **1996**, *28*, 731. (b) Eberhard, J.; Howard, C. J. *J. Phys. Chem. A* **1997**, *101*, 3360.

(6) Xing, J.-H.; Nagai, Y.; Kusuhara, M.; Miyoshi, A. *J. Phys. Chem. A* **2004**, *108*, 10458.

(7) Kondow, T. *J. Phys. Chem.* **1987**, *91*, 1307.

(8) Sander, S. P.; Friedl, R. R.; Ravishankara, A. R.; Golden, D. M.; Kolb, C. E.; Kurylo, M. J.; Huie, R. E.; Orkin, V. L.; Molina, M. J.; Moortgat, G. K.; Finlayson-Pitts, B. J. *Chemical Kinetics and Photochemical Data for Use in Atmospheric Studies*; JPL Publication 02-25; Jet Propulsion Laboratory: Pasadena, CA, 2003.

(9) Kee, R. J.; Rupley, F. M.; Miller, J. A. Chemkin-II: A Fortran Chemical Kinetics Package for the Analysis of Gas-Phase Chemical Kinetics, Sandia National Laboratories, Sandia Report: SAND89-8009B UC-706, 1986.

(10) Miyoshi, A.; Yamauchi, N.; Matsui, H. *J. Phys. Chem.* **1996**, *100*, 4893.

(11) Porret, D.; Goodeve, C. F. *Proc. R. Soc. London, Ser. A* **1938**, *165*, 31.

(12) Jung, K.-H.; Lee, C. M.; Yoo, H. S. *Can. J. Chem.* **1983,** *61*, 2486.

(13) Baboul, A. G.; Curtiss, L. A.; Redfern, P. C. *J. Chem. Phys.* **1999**, *110*, 7650.

(14) Frisch, M. J.; Trucks, G. W.; Schlegel, H. B.; Scuseria, G. E.; Robb, M. A.; Cheeseman, J. R.; Montgomery, Jr., J. A. T. Vreven, J. A.; Kudin, K. N.; Burant, J. C.; Millam, J. M.; Iyengar, S. S.; Tomasi, J.; Barone, V.; Mennucci, B.; Cossi, M.; Scalmani, G.; Rega, N.; Petersson, G. A.; Nakatsuji, H.; Hada, M.; Ehara, M.; Toyota, K.; Fukuda, R.; Hasegawa, J.; Ishida, M.; Nakajima, T.; Honda, Y.; Kitao, O.; Nakai, H.; Klene, M.; Li, X.; Knox, J. E.; Hratchian, H. P.; Cross, J. B.; Adamo, C.; Jaramillo, J.; Gomperts, R.; Stratmann, R. E.; Yazyev, O.; J. Austin, A.; Cammi, R.; Pomelli, C.; Ochterski, J. W.; Ayala, P. Y.; Morokuma, K.; Voth, G. A.; Salvador, P.; Dannenberg, J. J.; Zakrzewski, V. G.; Dapprich, S.; Daniels, A. D.; Strain, M. C.; Farkas, O.; Malick, D. K.; Rabuck, A. D.; Raghavachari, K.; Foresman, J. B.; Ortiz, J. V.; Cui, Q.; Baboul, A. G.; Clifford, S.; Cioslowski, J.; Stefanov, B. B.; Liu, G.; iashenko, A.; Piskorz, P.; Komaromi, I.; Martin, R. L.; Fox, D. J.; Keith, T.; Al-Laham, M. A.; Peng, C. Y.; Nanayakkara, A.; Challacombe, M.; Gill, P. M. W.; Johnson, B.; Chen, W.; Wong, M. W.; Gonzalez, C.; Pople, J. A. *Gaussian 03, Revision B.03*; Gaussian, Inc., Pittsburgh, PA, 2003.

(15) Ruiz, R. P.; Bayes, K. D. *J. Phys. Chem.* **1984**, *88*, 2592.

(16) Atkinson, R.; Baulch, D. L.; Cox, R. A.; Crowley, J. N.; Hampson, R. F.; Kerr, J. A.; Rossi, M. J.; Troe, J. *Summary of Evaluated Kinetic and Photochemical Data for Atmospheric Chemistry*, IUPAC, 2002. http://www.iupac-kinetic.ch.cam.ac.uk/.

(17) Anastasi, C.; Arthur, N. L. *J. Chem. Soc., Faraday Trans. 2* **1978**, *3*, 277.

(18) Heicklen, J. *Adv. Photochem.* **1988**, *14*, 177.

(19) Fittschen, C.; Frenzel, A.; Imrik, K.; Devolder, P. *Int. Chem. Kinet.* **1999**, *31*, 860.

(20) Balla, R. J.; Nelson, H. H.; McDonald, J. R. *Chem. Phys.* **1985**, *99*, 323.

(21) Le Calve, S.; Hitier, D.; Le Bras, G.; Mellouki, A. *J. Phys. Chem. A* **1998**, *102*, 4579.

(22) Miyoshi, A.; Matsui, H.; Washida, N. *J. Phys. Chem.* **1990**, *94*, 3016.

(23) Baulch, D. L.; Duxbury, J.; Grant, S. J.; Montague, D. C. *J. Phys. Chem. Ref. Data* **1981**, *10* (Suppl. 1), 1.

(24) Hippler, H.; Luu, S. H.; Teitelbaum, H.; Troe, J. *Int. J. Chem. Kinet.* **1978**, *10*, 155.

(25) Lenhardt, T. M.; McDade, C. E.; Bayes, K. D. *J. Chem. Phys.* **1980**, *72*, 304.

(26) Bethune, D. S.; Lankard, J. R.; Sorokin, P. P.; Schell-Sorokin, A. J.; Plecenik, R. M.; Avouris, Ph. *J. Chem. Phys.* **1981**, *75*, 2231.

(27) Lotz, Ch.; Zellner, R. *Phys. Chem. Chem. Phys.* **2000**, *2*, 2353.

(28) Tsang, W. *J. Phys. Chem. Ref. Data* **1990**, *19*, 1.